Open Access Full Text Article

ORIGINAL RESEARCH

Highly Ordered Nanotube-Like Microstructure on Titanium Dental Implant Surface Fabricated via Anodization Enhanced Cell Adhesion and Migration of Human Gingival Fibroblasts

Zhaoming Deng[1,2], Lerong Yu[1,2], Yishen Kuang[1,2], Ziyao Zhou[1,2], Xiangwei Li[1]

[1]Department of Stomatology, The Fifth Affiliated Hospital of Sun Yat-Sen University, Zhuhai City, 519000, People's Republic of China; [2]Guangdong Provincial Key Laboratory of Biomedical Imaging, The Fifth Affiliated Hospital of Sun Yat-Sen University, Zhuhai City, 519000, People's Republic of China

Correspondence: Xiangwei Li, The Fifth Affiliated Hospital of Sun Yat-Sen University, East Meihua Road No. 52, Xiangzhou District, Zhuhai City, Guangdong Province, People's Republic of China, Email lixiangwei@126.com

Background: Titanium (Ti) surface with nanotubes array via anodization has been used in dental implants to enhance bone regeneration but little research was carried out to evaluate whether the presence of highly ordered or disorderly distributed nanotubes array on titanium surface would have an effect on cell behaviors of gingival fibroblasts.

Methods: The present study fabricated nanotubes arrays with varied topography under different constant voltage of electrochemical anodization in fluorine-containing electrolyte. Human gingival fibroblasts (HGFs) from extracted third molar were harvested and co-cultured with titanium disks with different nanotubes topography. Then cell behaviors of gingival fibroblasts including cell proliferation, adhesive morphology and cell migration were estimated to investigate the influence of titanium nanotubes on cell biology. Besides, gene and protein expression of adhesion molecule (integrin $\beta1/\beta4/\alpha6$, fibronectin, intracellular adhesion molecule-1 and collagen type I) were detected to evaluate the influence of different surfaces on cell adhesion.

Results: Highly ordered arrays of nanotubes with pore diameter of 60 nm and 100 nm were fabricated under 30 and 40 V of anodization (TNT-30 and TNT-40) while disorderedly distributed nanotube arrays formed on the titanium surface under 50 V of anodization (TNT-50). Our results demonstrated that compared with raw titanium surface and disorderly nanotubes, surface with orderly nanotubes array increased cell area and aspect ratio, as well as cell migration ability in the early phase of cell adhesion ($p<0.05$). Besides, compared with raw titanium surface, gene and protein expression of adhesion molecules were upregulated in nanotubes groups to different extents, no matter whether in an orderly or disorderly array.

Conclusion: Within the limitations of our study, we conclude that compared with raw titanium surface, the presence of nanotubes array on titanium surface could enhance cells adhesion and cell migration in the early phase. And compared with disorderly distributed nanotubes, highly ordered nanotubes array might provide a much more favorable surface for gingival fibroblasts to achieve a tight adhesion on the materials.

Keywords: nanotubes, gingival fibroblast, cell behaviors, cell adhesion, gingival sealing

Introduction

Dental implants have been an effective treatment for patients who lose their teeth. As the major material, titanium and its alloy have a great biocompatibility with the adjacent hard tissue, guaranteeing a desirable osseointegration in the alveolar bone. Similar to natural teeth, there is a circular part on the implant or implant abutment surface that penetrates oral mucosa, which requires tight soft tissue sealing to protect against pathogenic microorganisms from the oral environment.[1] A deficient gingival sealing around the implant surface might be a contributing factor to the invasion of pathogenic bacteria from the oral cavity, which gives rise to peri-implant diseases including peri-implant mucositis and peri-implantitis.[2,3] Unlike the tight gingival

Graphical Abstract
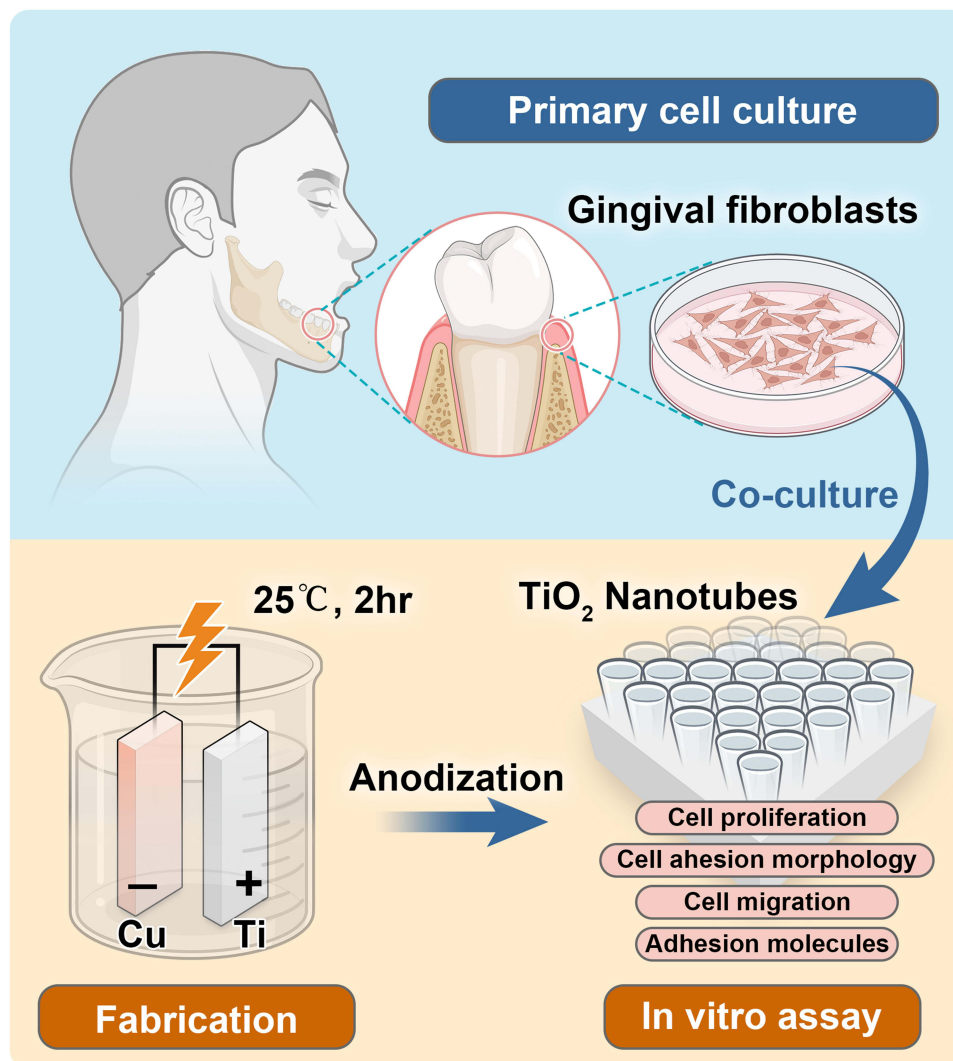
sealing around natural teeth with the help of high expression of adhesion structure hemidesmosomes (HD) and the Sharpey's fibers perpendicularly inserting to cementum, peri-implant sealing is comparatively weakened due to the limited adhering interface where adhesion structures could be observed, and to the failure of rehabilitation of perpendicular collagen fibers.[4,5]

There are studies reporting a variety of methods to modify the implant surface with an aim of increasing soft tissue adhesion to the implant.[6–8] For example, though not fully understood, it was increasingly observed and recognized that a highly polished surface enhanced epithelial attachment and fibroblasts adhesion, compared with the rough surface which might on the other hand appeal to microorganisms from the oral environment.[9,10] Also, abutment surface could be physically coated by various biological macromolecules such as chitosan, collagen, and gelatin.[11–13] These kinds of natural coating were integrated on the surface to increase protein adhesion and thereafter enhance the attachment of gingival epithelial cells and fibroblasts. However, the uncontrolled degradation rate of these natural components set a challenge to the clinical transformation in the long term. Therefore, more and more direct surface modifications were introduced and explored to enhance gingival sealing of dental implant abutment, such as the nanoscale fabrication of grooves, pores, and tubes on titanium surface.[14–16]

Among various methods, nanotubes fabricated by electrochemical anodization (EA) is attracting increasing attention in implant surface modification due to its easy processing and preparation, and the varied biological effect brought by different topographical characteristics of nanotubes.[17] Dental implants with nanotubes made by anodization have been widely accepted and proven to have an enhancing effect on bone regeneration around the implant.[18–21] The internal space with only one opening inside the nanotube enables the incorporation of various kinds of biological molecules, which might have various promising application including controlled drug release, antibacterial activity, and immune microenvironment regulation.[22–24] There are studies reporting that topographical features of nanotubes could reduce the macrophage inflammatory response and stimulate macrophage toward M2 phenotype-polarization, creating a pro-healing immune microenvironment to initiate wound recovery.[25,26] Gao et al, incorporated nanostructured implant surface with silver and found enhanced inflammatory responses in vivo.[21] Recently, increasing research has been carried out to evaluate the biological effect of titanium surface with nanopores or nanotubes made by electrochemical anodization on gingival fibroblasts and epithelial cells which are sensitive to surface characteristics such as chemical and physical features.[27–29] Gulati et al, found the presence of nanopores with small diameter of 40–70 nm exhibited robust effect for gingival fibroblast to grow and adhere to the surfaces.[30] Ferrá-Cañellas et al, aimed their work to evaluate how tuning the size of nanopores could benefit gingival fibroblasts.[31] Besides, Wang et al, emphasized in their work how hydrophilicity of the nanotube-containing titanium surface could influence cell behavior of gingival fibroblasts.[32]

The present work was initiated to evaluate whether the presence of nanotubes fabricated via electrochemical anodization on the surface of titanium could influence cell behaviors of gingival fibroblasts, and to determine what different topographical characteristics and array feature of nanotubes influence cell morphology and accordingly cell adhesion ability on the surface.

Materials and Methods
Ethical Approval and Informed Consent
The present study complied with the Declaration of Helsinki and was approved and monitored by the ethics committee of the Fifth Affiliated Hospital of Sun Yat-sen University with ethical approval reference [2023-K207-1]. Informed consent was attained from the donors before the use of gingival fibroblasts.

Titanium Disks Preparation
Raw commercially purchased titanium round disks (diameter of 8.0 mm, thickness of 0.43 mm) were bought from Anyou Xincai Co, Ltd. All Ti disks were cleaned by acid mixture solution (1M hydrofluoric acid (HF) 1M nitric acid) under vigorous oscillation for 2 min, after which the disks were further cleaned successively by acetone, ethanol, and deionized water. The surface of titanium disks was then polished by finishing bur in a low-speed drilling of 9000 rpm. All the disks were successively cleaned again by acetone, ethanol, and deionized water before electrochemical anodization (EA).

Electrochemical Anodization (EA)
To fabricate nanotubes (TNT) with different diameter on the surface of Ti disk, different EA duration, and voltage were explored in our previous study. 70 v/v% ethylene glycol (containing 0.25 wt% ammonium fluoride (NH_4F)) was considered as feasible electrolyte to modify the titanium surface. To explore the impact of EA time and voltage, Ti disks were anodized for 2 min, 10 min, 30 min, 1 hr, 2 hr, and 4 hr under constant voltage of 30, 40, 50, and 60V respectively. Copper was chosen as cathode. All the disks were successively cleaned by acetone, ethanol, and deionized water after EA.

Surface Characterization
Surface topography, roughness and chemical features of the Ti disks used in this study were characterized. Anodized or raw titanium (RT) disks were dehydrated via vacuum dryer and gold-sputtered before observation under scanning electron microscope (SEM) (Phenom Scientific, China). The surface of titanium disks was observed in backscatter diffraction (BSD) mode or secondary electron detection (SED) mode under accelerating voltage of 10 kV and at 50 k magnification.

Surface roughness was estimated by atomic force microscope (Bruker Dimension Icon, Germany). The average roughness measurements were determined at three locations for each disk. Chemical characteristics of the surface of titanium disks was determined by energy dispersive X-ray spectrometry (EDS) (Phenom Scientific, China).

Primary Cell Culture

Small pieces of gingival tissue from freshly extracted third molar were collected and washed by saline solution containing 100 μg/mL penicillin/streptomycin (Thermo Fisher Scientific, MA, USA). Gingival tissue was cut and minced to 1.0 mm^3, then incubated in digesting mixture containing 8 mg/mL neutral proteases and 6 mg/mL collagenase for 1 hr at 37°C. Gingival cells suspension was added in Minimum essential medium-α (MEM-α) medium (Thermo Fisher Scientific, MA, USA) consisting of 10% fetal bovine serum (FBS) (Thermo Fisher Scientific, MA, USA) and 100 μg/mL penicillin/streptomycin (Thermo Fisher Scientific, MA, USA). Gingival fibroblasts were harvested and amplified by single cell colony methods. Cell culture was maintained at 37°C with 5% CO_2 in a humidified incubator before the following experiments.

Identification of Gingival Fibroblasts

The identification of gingival fibroblasts was carried out by indirect immunofluorescence staining of vimentin and CD90 which are mostly expressed by fibroblasts. 5×10^3 cells were seeded on the coverslip and after 2 d of culture fixed with 4% (w/v) paraformaldehyde (PFA, Thermo Fisher Scientific, USA) for 20 min. Then, HGFs were permeabilized with 0.5% (v/v) Triton X-100 (Solarbio, Beijing, China) for 10 min and blocked with 5% (w/v) bovine serum albumin (BSA; Sigma Aldrich, USA) for 1 h at room temperature. HGFs were labeled with vimentin (1:200 dilution, #60330-1-IG, Proteintech, China) and CD90 (1:250 dilution, 27178-1-AP, Proteintech, China) diluted in 1% (w/v) BSA and incubated overnight at 4°C. In the second day, HGFs were incubated with secondary antibody Alexa Fluor 488 (for vimentin, 1:500 dilution, #ab150080, Abcam, UK) and Alexa Fluor 594 (for CD90, 1:500 dilution, #ab150080, Abcam, UK) for 1 hr at room temperature. Finally, samples were mounted in antifade reagent with DAPI (P0126-5mL, Beyotime, China) and observed under immunofluorescence microscope.

Flow cytometry was performed to confirm the expression of the surface markers CD10, CD63, CD24, and CD326. 1×10^6 of HGFs at the third passage were incubated with the fluorescently labeled antibodies APC Mouse Anti-Human CD10 (#340923), FITC Mouse Anti-Human CD63 (#550759), BV786 Mouse Anti-Human CD24 (#568225) and PE Mouse Anti-Human CD326 (#566841) (1:20 dilution, all from BD Pharmingen, USA) for 15 min at 4°C in the dark, after which cells were washed with 3 mL of PBS containing 2% FCS and centrifuged at 4°C, 1300 rpm for 5 min. Subsequently, the supernatant was discarded and cell pellet was dissolved in 100 μL PBS with 2% FCS. The labeled cells were analyzed using a BD FACSCanto II (BD Biosciences, USA) and the Flow cytometry data were analyzed via FCS Express 7 (De Novo Software, USA).

Cell Proliferation Estimation

Raw Ti and TNT disks were disinfected and uviolized before cell seeding. HGFs were harvested and seeded on each disk with the density of 2500 cells, and cultured for 1/4/7 days. Indirect immunofluorescence assay was used to evaluate the cell proliferation. At each endpoint of cell culture, HGFs were fixed with 4% paraformaldehyde (Bioss, Beijing, China). Then cells were permeated with 0.3% Triton X-100 and blocked with 5% (w/v) bovine serum albumin (BSA; Sigma Aldrich, USA) for 1 hr at room temperature. Samples were then mounted in antifade reagent with DAPI (P0126-5mL, Beyotime, China). Images were captured via confocal laser scanning microscopy (LSM880, Zeiss, Germany). In the captured images, each blue dot of DAPI represented a single cell. The cell count was represented by the nucleus count at each timepoint.

Cell Adhering Morphology

Cell adhering morphology on the surface of the disks was evaluated by immunofluorescence and SEM. HGFs were seeded on each disk with the density of 1000 cells and cultured for 6 hr, 12 hr, 1 d and 4 d.

For immunofluorescence, cells were fixed with 4% paraformaldehyde at each timepoint of cell culture. Then the cells were permeated by 0.3% Triton X-100 for 15 min and consecutively washed by saline three times (each for 5 min). After

blocking with 5% (w/v) bovine serum albumin (BSA) for 1 hr at room temperature, cells were incubated for 30 min at room temperature with 488-conjugated Phalloidin (#23115, AAT Bioquest, US) to stain the cytoskeleton. DAPI was used to stain the cell nucleus in the final step. Images were captured via a confocal laser scanning microscopy (LSM880, Zeiss, Germany). Three fields under microscope were chosen randomly and average cell area and cell aspect ratio was calculated via imageJ software (1.53v, National Institutes of Health, USA). Cell area was directly measured using area calculating module of imageJ, and cell aspect ratio was determined by cell length divided by its width.

For SEM, HGFs were fixed with 2.5% glutaraldehyde and then dehydrated in graded ethanol (50%, 70%, 80%, 90%, 100%, and another 100%, each for 20 min) with constant oscillation. The dehydrated specimens were incubated in hexamethyl disilylamine (HMDS) for 10 min before vacuum desiccation overnight at 40°C. All the specimens were sputter-coated with gold and observed via the scanning electron microscope (Phenom, Thermo Fisher Scientific Inc., USA) in backscatter diffraction (BSD) mode or secondary electron detection (SED) mode under accelerating voltage of 10 kV and at 50 k magnification.

Cell Migration Assay

Wound healing assay was used to evaluate cell migration ability on the surface of titanium disks. HGFs were seeded and cultured on the disks. After cell confluency reached 90%, a straight scratch was made by using 200 μL pipette tip on the surface of the disks to simulate a wound. Cells were continuously cultured in medium containing only 1% FBS for 1 and 2 days to preclude cell proliferation effect. At the time of scratch-making, 1-day culture and 2-day culture, cells were fixed with 4% paraformaldehyde for 15 min at room temperature. Then the cells were permeated by 0.3% Triton X-100 for 15 min and consecutively washed by saline three times (each for 5 min). After blocking with 5% (w/v) bovine serum albumin (BSA) for 1 hr, cells were incubated at room temperature for 30 min with 488-conjugated Phalloidin (#23115, AAT Bioquest, US). DAPI was used to stain the nucleus. Images were captured via a confocal laser scanning microscopy (LSM880, Zeiss, Germany). In the captured images, HGFs moving to the central blank space originally made by pipette tip were seen as endocentrically migrated cells. Cell migration percentage was represented by the endocentric area of the migrating cells.

Reverse Transcription (RT) and Quantitative Real-Time PCR (qPCR)

To evaluate the expression of molecules relating to cell adhesion on different groups, total RNA was extracted from samples using RNA-easy Isolation Reagent Kit (#R701-01, Vazyme, China), and reverse transcription was performed to prepare cDNA. Quantitative real-time PCR was performed using specific primers, including ITGA6 (integrin α6), ITGB4 (integrin β4), COL-1 (collagen type 1), FN (Fibronectin), ICAM-1 (intercellular cell adhesion molecule-1), and ITGB1 (integrin β1), (sequences shown in Table 1). GAPDH was selected as an internal control, and mRNA expression of all samples was standardized to that of GAPDH.

Table 1 Primer Sequences

Gene	Forward Primers (5 ′to 3 ′)	Reverse Primers (5 ′to 3 ′)
ITGA6	CGAAACCAAGGTTCTGAGCCCA	CTTGGATCTCCACTGAGGCAGT
ITGB4	AGGATGACGACGAGAAGCAGCT	ACCGAGAACTCAGGCTGCTCAA
COL-1	TCTAGACATGTTCAGCTTTGTGGAC	TCTGTACGCAGGTGATTGGTG
FN	TTTTAAGCTGGGTGTACG	CAAGTTTGTTGGTGGAGA
ICAM-1	AGCGGCTGACGTGTGCAGTAAT	TCTGAGACCTCTGGCTTCGTCA
ITGB1	TGTGTCAGACCTGCCTTGGTG	AGGAACATTCCTGTGTGCATGTG
GAPDH	GCACCGTCAAGGCTGAGAAC	TGGTGAAGACGCCAGTGGA

Western Blotting

Western blotting was performed to detect the expression of proteins related to cell adhesion. Total proteins were extracted from cells of each group using RIPA lysis buffer (Beyotime, Shanghai, China). A BCA protein assay kit (Beyotime, Shanghai, China) was used to measure the concentration of harvested proteins. An equal amount of 25 μg protein of each group was subjected to SDS-PAGE, followed by blotting onto a polyvinylidene difluoride (PVDF) membrane (Millipore, MA, USA). After blocking with 10% skimmed milk, the membrane was probed overnight at 4°C using specific primary antibodies including integrin β1 (26918-1-AP,1:1000, ProteinTech, China), Fibronectin (15613-1-AP, 1:1000, ProteinTech, China), Integrin α6 (27189-1-AP, 1:1000, ProteinTech, China), and Integrin β4 (21738-1-AP, 1:1000, ProteinTech, China), followed by incubation with a horseradish peroxidase–conjugated secondary antibody, HRP-goat anti-mouse or HRP-goat anti-rabbit, for 1 hr at room temperature. The signal was visualized with a SuperKine™ West Femto Maximum Sensitivity Substrate (BMU102-CN, Abbkine) using Invitrogen iBright CL1500 imaging system (Thermo Fisher Scientific, USA). Bands data from Western blot were analyzed via iBright Analysis Software (5.2.2, Thermo Fisher Scientific, USA).

Statistical Analysis

All the numerical data were presented as mean ± standard deviation (SD) and analyzed using IBM SPSS 17.0 (Armonk, NY, USA). The diameter of nanotubes was calculated by Origin Pro (OriginLab, USA). One-way analysis of variance (ANOVA) followed by LSD test were used to compare the variation among different groups. P value <0.05 was considered to be statistically significant. All experiments were performed in triplicate.

Results

Nanotubes Topography Was Dependent on Voltage and Anodizing Duration

Different topography of nanotubes could be fabricated on the polished titanium surface under different anodized duration and voltage (Supplementary Figure). Generally, pore-like structures (nanopores) formed at first (within 30 minutes) on the surface under 30, 40 and 50 V. With anodizing time increased, nanopores gradually grew and turned to be tube-like structures (nanotubes). For 30 and 40 V, the distribution and diameter of nanotubes become evenly ordered after 1 hr duration (Supplementary Figure A–L). For 50 V, nanotubes formed at 2 hr duration (Supplementary Figure M–R), but the nanotubes presented disordered and varied in diameter. For 60 V, no nanotube was fabricated on the surface (Supplementary Figure S–X) from 2 min to 2 hr. After 4 hr duration, disorderly distributed nanotubes were presented on the surface and the diameter of the nanotubes varied in size greatly.

In the present study, preparation of 30.40 and 50 V with 2 hr duration were selected for optimal fabrication of nanotubes on the surface of raw titanium (RT). As shown in Figure 1, the results of the top view of SEM demonstrated that the surface of RT presented a ridge-like topography while titanium nanotubes (TNT) could be integrated on the surface of RT, with varied topographical features due to the differences of anodizing parameter (Figure 1A–D). The 45° tilt view of SEM confirmed the tube-like structure which also presented parameter-dependent configuration (Figure 1E–H). Dense and orderly distributed nanotubes were seen on the surface of TNT-30 and TNT-40 (Figure 1F and G) while the nanotubes on the surface of TNT-50 presented to be cone-like structure and the distribution of the nanotubes was looser and much more disordered (Figure 1H).

The results of energy dispersive spectrum (EDS) analysis confirmed that the introduction of oxygen into the nanotubes and no impurities were brought in from the anodizing process (Figure 1I–M). Diameter of the nanotubes was measured and the results showed that the mean diameter of nanotubes of TNT-30 was 61.4±2.4 nm while the mean diameter of nanotubes of TNT-40 was 103.4±2.5 nm (Figure 1N and O). However, the measured diameter of nanotubes in TNT-50 presented abnormal distribution and the mean diameter of nanotubes could not be measured precisely (Figure 1P). Roughness analysis showed that the fabrication of orderly distributed nanotubes on the Ti surface (TNT-30 and TNT-40) significantly increase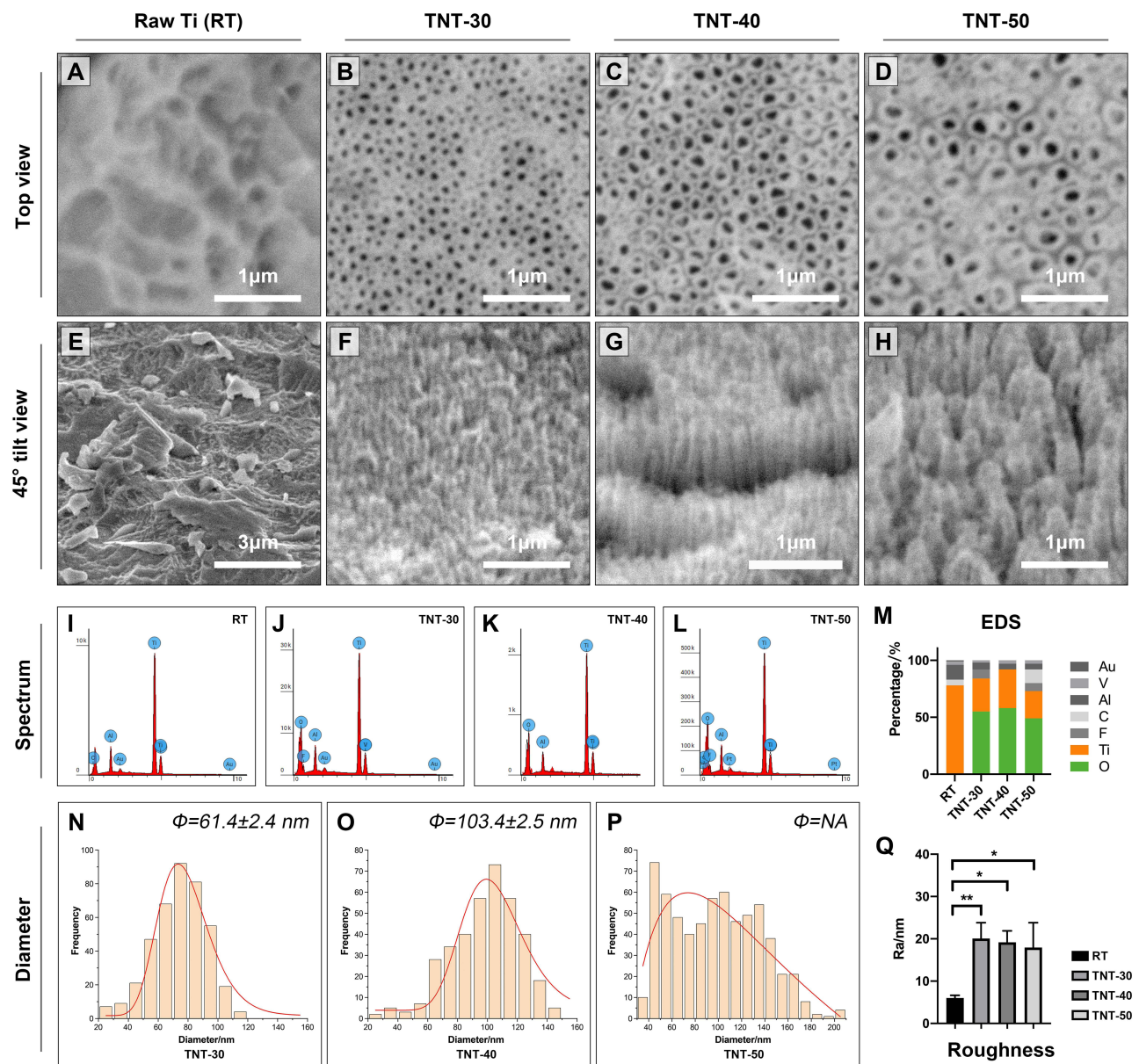d the roughness of the surfaces, compared with RT ($p<0.05$) and no difference in roughness was found between TNT-30/40/50 ($p>0.05$).

Figure 1 The topographical, chemical, and roughness features of raw titanium (RT) and TNT-30/40/50. Top view (**A–D**) and 45° tilt view (**E–H**) of the surfaces showed that there were ridge-like structures on the surface of RT while nanotubes with varied diameter and distribution were fabricated on titanium surfaces. Energy dispersive X-ray spectrometry (**I–L**) showed the chemical composition of each sample. Raw titanium consisted of elements including titanium (Ti), aluminum (Al), carbon (**C**), vanadium (**V**), and gold (Au). After anodization in fluoride-containing electrolyte, oxygen (**O**) and fluorine (**F**) were introduced (panel **M**). Mean diameter of nanotubes was measured in TNT-30 and 40, which were 61.4±2.4 nm and 103.4±2.5 nm (**N** and **O**). However, tubes diameter varied greatly in TNT-50 and the tubes distribution was abnormal, for which reason mean diameter of the nanotubes could not be measured (**P**). Besides, compared with RT, the fabrication of nanotubes array (TNT-30/40/50) increased the roughness of titanium surface (**Q**). (******Represents p<0.01, *Represents p<0.05, both are compared with RT).

Human Gingival Fibroblasts Were Identified via Indirect Immunofluorescence and Flow Cytometry

Gingival cells were isolated and cultured (Figure 2A). Typical spindle shaped morphology could be observed under bright field images (Figure 2B). Identification of fibroblasts was carried out via indirect immunofluorescence staining of vimentin and CD90 (Figure 2C and D), which were considered as typical markers expressed by fibroblasts. Besides, flow cytometry results also demonstrated that the harvested and analyzed cells highly expressed fibroblastic markers CD63 and CD10, whereas the expression of epithelial markers CD326 and CD24 were undetectable (Figure 2E–G). All these results could confirm the cells we isolated and cultured were human gingival fibroblasts (HGFs).
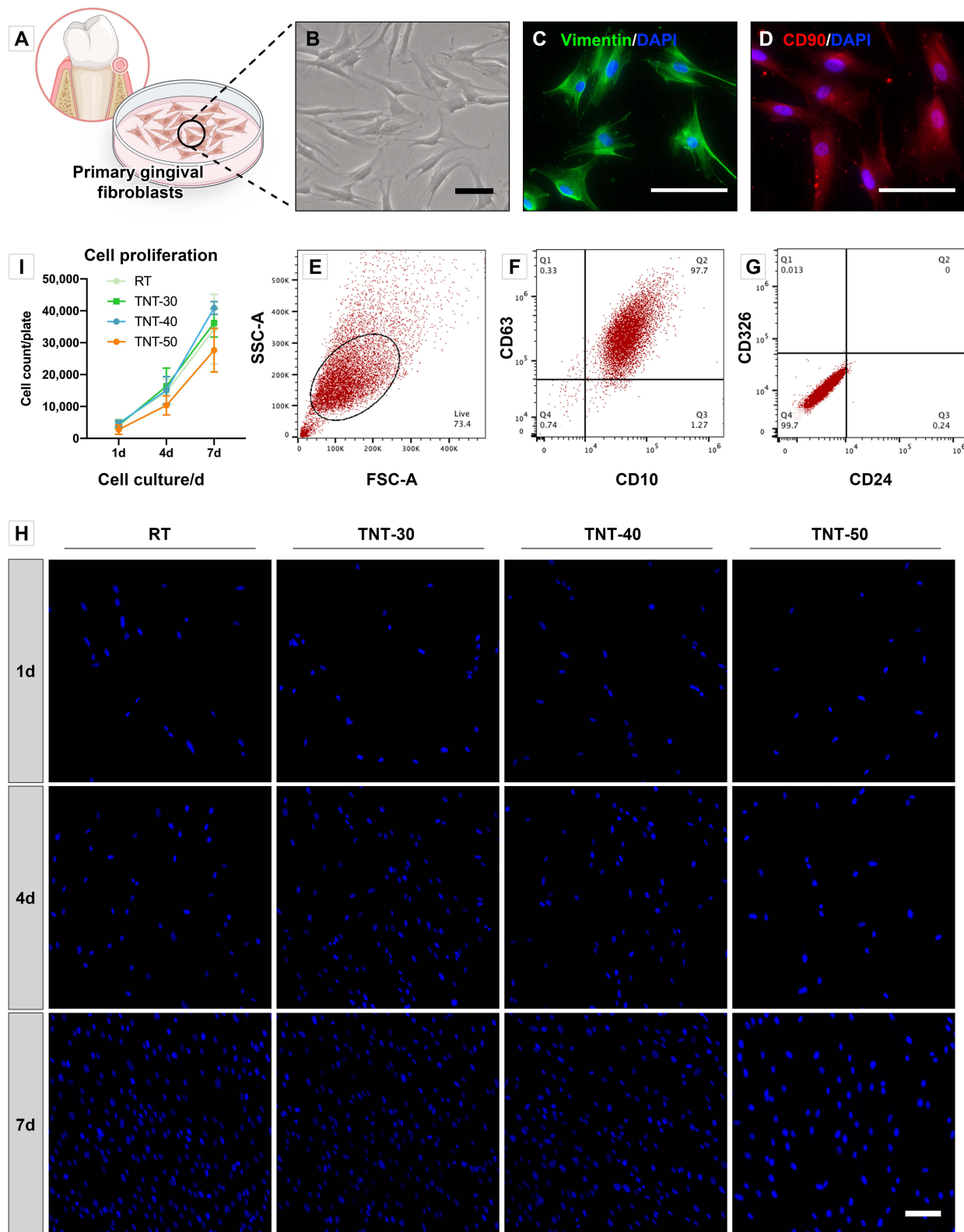
Figure 2 Cell identification and proliferation estimation of human gingival fibroblasts. Primary gingival fibroblasts were isolated from healthy gingiva of donor and cultured carefully (**A**). Typical spindle-shaped morphology of human gingival fibroblasts was observed under bright field image (**B**). Vimentin (**C**) and CD90 (**D**) expression of HGFs was visualized by indirect immunofluorescence assay. Forward scatter (FSC-A) plot against side scatter (SSC-A) plot was used to gate fibroblasts and to exclude cell debris (**E**). CD10 and CD63 served as positive markers of HGFs with 97.7% of gated cells (**F**) while CD24 and CD326 served as negative markers (**G**). Equal amount of HGFs were seeded on the surface of Ti disks of different groups (RT/TNT-30/TNT-40/TNT-50) and grew on consecutive 1/4/7 days (**H**). One blue dot of DAPI represented a single cell of fibroblast. The results of cell counts showed that there was no significant difference in aspect of cell proliferation between groups at each timepoint, indicating the favorable biocompatibility of nanotubes array on titanium surface (**I**). (Scale bar = 100 μm in **B, C, D**, and **H**).

Titanium Nanotubes Topography Exerted No Cytotoxicity to HGFs

HGFs were seeded on the surface of each group. The results of cell count under fluorescence microscopy demonstrated that HGFs seeded on the Ti disks of all groups presented unaffected cell proliferation (Figure 2H). And there was no significant difference between groups in aspects of cell proliferation (Figure 2I). The results indicated that the fabrication of nanotubes array on the surface of titanium disks did not compromise cell proliferation and exerted no cytotoxicity to the gingival fibroblasts.

TNT-30 and TNT-40 Increased Cell Spread in the Early Phase

The ability of cell spread was evaluated by measuring the adhering cell area and aspect ratio of gingival fibroblasts cultured in different groups for 6 hr, 12 hr,1 d and 4 d, respectively (Figure 3). At the 6th hour of culture, cells of all groups presented similarly round shape and no significant difference was seen between groups in cell area and aspect ratio (Figure 3A–D). Later at the 12th hour of culture, HGFs cultured on TNT-40 surface extended much longer protrusions compared with other groups (Figure 3E–H). On the contrary, the morphology of HGFs cultured on TNT-50 surfaces did not change at the 12th hour (Figure 3H). Then on the first day of culture, aspect ratio of HGFs cultured on TNT-30 and TNT-40 increased significantly (Figure 3I–L and R) ($p<0.01$), compared with RT and TNT-50. At this timepoint, it was also shown that fibroblasts on TNT-40 presented the largest cell area compared with other groups (Figure 3Q). On the 4th day of the culture, fibroblasts of all groups presented no difference in cell area and aspect ratio (Figure 3M–P).

TNT-30 and TNT-40 Increased Cell Protrusion on the Ti Disks

Cell morphology was also evaluated via SEM. Similarly, at the 6th hour of cell culture, HGFs did not spread to spindle shaped and were seen to be round shaped in all groups (Figure 4A–D). However, HGFs seeded on the surface containing nanotubes (TNT-30/40/50) started to extend more pseudopodia to the surface of the Ti disks (details shown in Figure 4A1–D1), compared with the fibroblasts on the RT surface. On the first day of cell culture, spindle-like cell morphology was observed on TNT-30 and TNT-40, while cells on RT and TNT-50 did not fully spread (Figure 4E–H). The fabrication of tube-like structures on titanium surface enables HGFs to extend tiny cell protrusions into the hollow space of the nanotubes, compared with cells on RT which lack this kind of interaction with the surface of the materials (Figure 4I–L).

Titanium Nanotubes Enhanced Fibroblast Migration

Wound healing assay was selected to evaluate cell migration of gingival fibroblasts in contact with titanium disk with different topography (Figure 5). At the first day, compared with RT, the presence of nanotubes on titanium surface enhanced cell migration to different extent. It was noteworthy that tube diameter of approximately 100 nm (TNT-40) had the greatest effect on cell migration compared with other groups ($p<0.05$) (Figure 5A–H). Later on day 2 of cell migration, fibroblasts on TNT-30 and TNT-40 presented greater migration ability compared with RT and TNT-50 ($p<0.05$) (Figure 5I–M). The present results indicated that the fabricated nanotubes on the surface of titanium could enhance cell migration of gingival fibroblasts, and the tubes with diameter of 60 and 100 nm might have the most promising effect.

Titanium Nanotubes Increased the Expression of Molecule Related to Cell Adhesion

mRNA and protein expression at three different timepoints were detected and quantified via quantitative real-time PCR and Western blotting. Overall, HGFs seeded on nanotube-containing surfaces, no matter what topography, presented higher expression in gene level of molecules related to cell adhesion such as ITGB1, FN, ITGA6, ITGB4, ICAM-1 and COL-1, compared with raw Ti surface ($p<0.05$) (Figure 6A). Meanwhile, the results also indicated that orderly-distributed nanotubes surface (TNT-30 and TNT-40) increased much more expression of cell-adhesion-related gene, compared with TNT-50 representing disorderly-distributed nanotubes surface. The results of protein expression of adhesive molecule demonstrated that compared with the raw Ti, the presence of nanotubes on the surface exerted a positive role in regulating cell adhesion (Figure 6B), especially the expression of integrin β1 and fibronectin at all timepoints of cell culture (Figure 6B). The presence of nanotubes surface increased the expression of integrin α6 at the
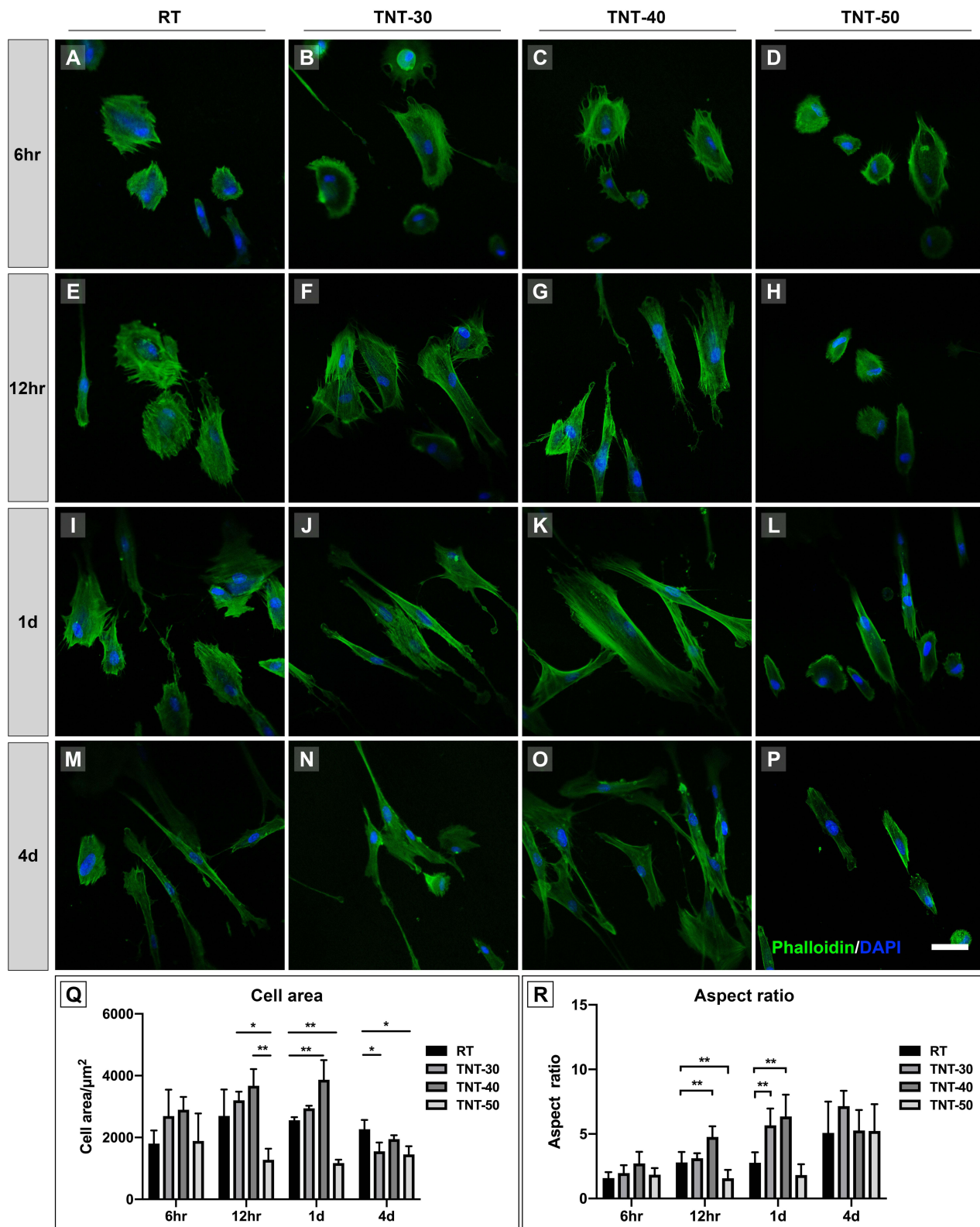
Figure 3 Adhesive morphology of HGFs was visualized with phalloidin staining (Green) under immunofluorescence microscopy. Fibroblasts were round shaped and started to spread with pseudopodia at 6 hr of culture on the surfaces (**A–D**). At this timepoint, there was no significant difference between groups in cell area and aspect ratio. At 12 hr, HGFs on TNT-40 surface showed increased cell area compared with other groups (**E–H**) and demonstrated significantly increased aspect ratio compared with RT ($p<0.01$), while HGFs on TNT-50 surface showed the least in cell area and aspect ratio. At 1d of culture, cells of all nanotube groups (TNT-30/40/50) were spindles shaped, and cell aspect ratios of TNT-30 and TNT-40 were significantly increased compared with RT and TNT-50 ($p<0.01$) (**I–L**). At 4 d of cell culture, no significant difference in aspect ratio was seen between groups (**M–P**). Statistical analysis was shown in (**Q**) and (**R**). (Scale bar = 50 μm in all panels) (******Represents $p<0.01$, *****Represents $p<0.05$, both are compared with RT).
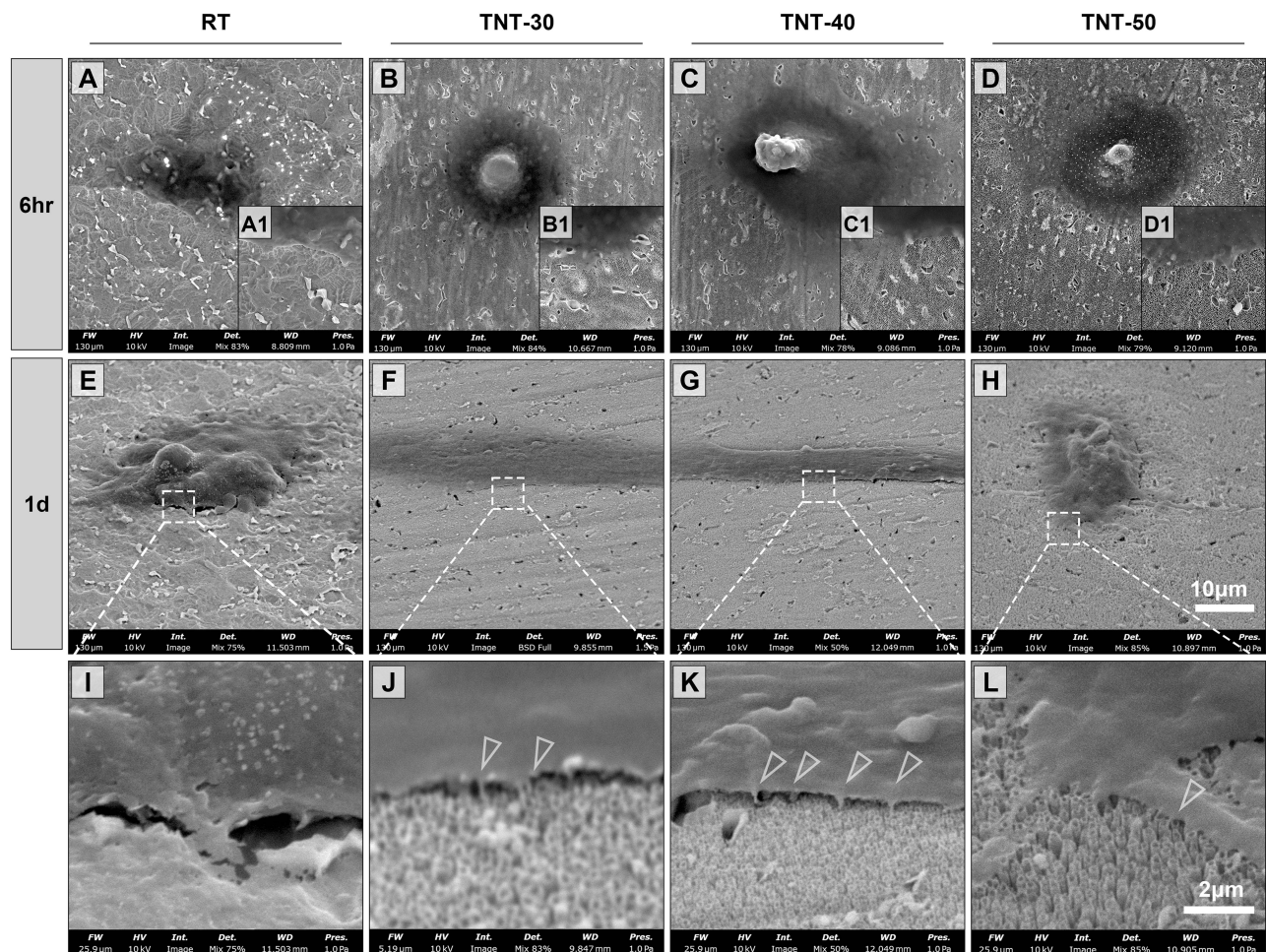
Figure 4 Representative SEM images illustrating adhesive morphology of HGFs on different surfaces. At 6 hr of cell culture, though still round-shaped, compared with RT, HGFs on nanotubes array (TNT-30/40/50) appeared to have plenty of pseudopodia extending from cell membrane (**A–D**, pseudopodia details in **A1–D1**). Later at 1 d of cell culture, compared with HGFs whose morphology have not fully spread on RT and TNT-50 (**E** and **H**), cells on TNT-30 and 40 spread terminally and turned to be spindle shaped (**F** and **G**). In higher magnification of dotted squares in panel (**E–H**), HGFs extended tiny protrusions (triangles in panel **J–L**) into the holes of the nanotube-containing surfaces (**I–L**).

initial 6th hour and integrin β4 at the 12th hour. At other timepoints, protein expression of integrin α6 and β4 was not significantly altered between groups. The semi-quantification of protein expression was presented in Figure 6C.

Discussion

A tight gingival sealing around dental implant abutment has been a requisite against the invasion of oral pathogenic organisms. Compared with the presence of cementum which could anchor the perpendicularly inserted fibers from periodontal ligament (Sharpey's fibers) and gingiva, collagen fibers in the connective tissue run circularly around the dental implant abutment without any surface modification, compromising gingival sealing efficacy.[5] For this reason, there is increasing researches focusing on surface modification in an aim of improving gingival adhesion and sealing on the implant abutment, especially in a bionic pattern.[30,33]

Among various modifications, fabrication of nanotubes on titanium surface is attracting increasing attention in recent years. Nanotubes topography (diameter, height, and array) could be easily designed by changing anodizing parameters such as the type of electrolyte, processing time, and anodizing voltage (Supplementary Figure). In the present study, we fabricated three types of nanotubes on titanium surface, representing highly ordered nanotubes array with two different tube diameter (~60 nm of TNT-30 group, ~100 nm of TNT-40 group) (Figure 1N and O), and one group of disordered nanotube array with abnormal distribution of tubes diameter (TNT-50) (Figure 1P). We aimed this study to
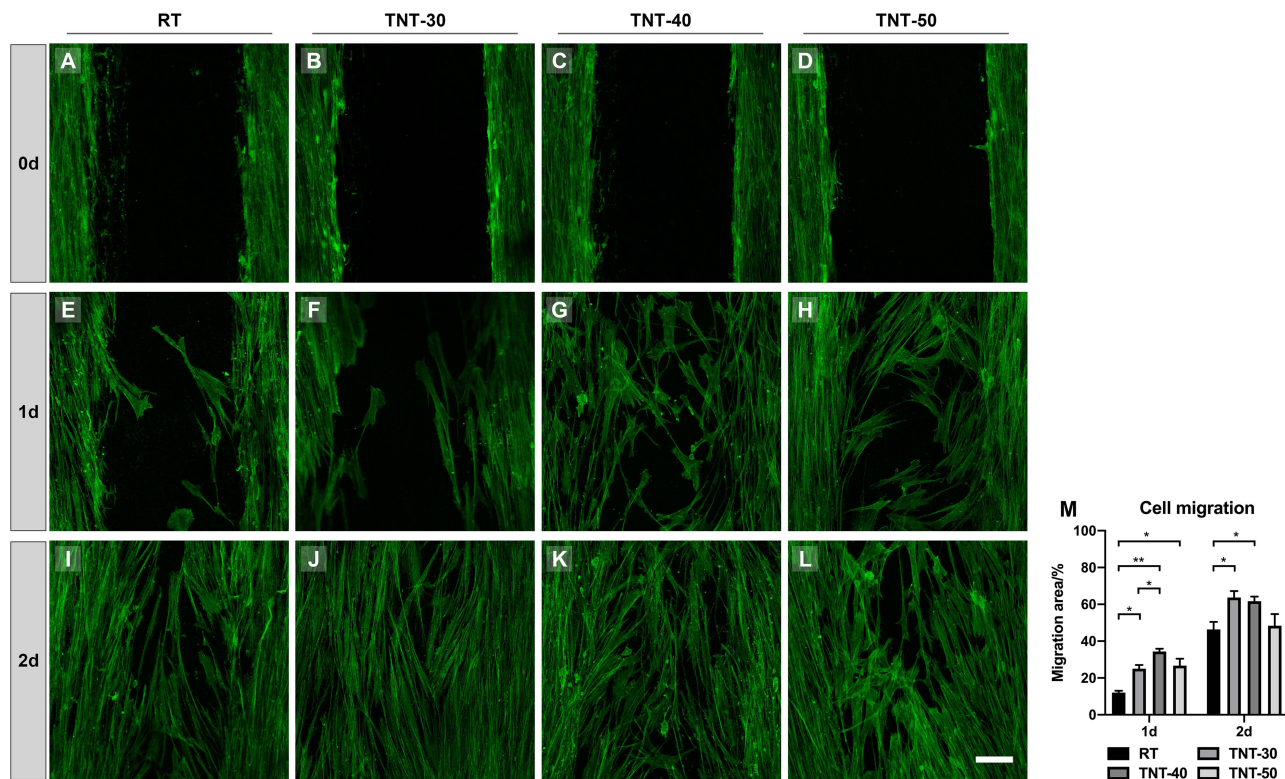
Figure 5 Cell migration assay on titanium disks with different morphology. A straight scratch was made by using 200 μL pipette tip on the surface of the disks to simulate a wound (**A–D**) and at the first day of cell culture (**E–H**), HGFs on nanotubes array (TNT-30/40/50) showed significantly increased migration area compared with RT (p<0.05) (**M**). At this timepoint, TNT-40 demonstrated the highest increased cell migration ability compared with RT, TNT-30, and TNT-50. Later at the second day of cell migration, HGFs on TNT-30 and TNT-40 presented greater migration ability compared with RT and TNT-50 (p<0.05) (**I-L**). (Scale bar = 100 μm in all panels) (**Represents p<0.01, *Represents p<0.05).

evaluate whether the presence of nanotubes on Ti surfaces could influence cell behaviors of gingival fibroblasts and to determine what kind of topographical features could enhance cell adhesion on the titanium surface after modification.

Cell counts on a consecutive day were carried out to evaluate cell proliferation cultured on the surface, representing the biocompatibility of the surface and the fabrication of nanotubes did not compromise cell proliferation and was proven to be perfectly compatible to gingival fibroblasts (Figure 2H and I). Also, it has been widely accepted that early cell adhesion on the surface in the initial stage plays an important role in the wound healing process.[34,35] Cells of all kinds should undergo several stages one by one before finally physically adhering to the surface, including contact, recognition, intracellular molecular response, and morphological change.[36] Highly ordered nanotubes array stimulated early cell spread on the surface and fast transformation to spindle shape (12 hr and 1 d) (Figure 3Q and R), compared with raw Ti surface and disordered surface (TNT-50). Aspect ratio was dependent on how long cell protrusions could be extended, which is a representative feature of cell adhesion. The presence of orderly array of nanotubes elongated cell protrusions compared with raw Ti surface, while disorderly nanotubes array adversely weakened cell extension on the surface in the early stage (6 hr, 12 hr, and 1 d). At the late stage of adhesion (4 d), cells of all groups presented full spread and cell extension (Figure 3). Besides, active cells would extend tiny protrusions from cell membrane to contact the surface as much as possible. Gingival fibroblasts on surface containing nanotubes array (TNT-30/40/50) extended much more pseudopodia to contact the surface (Figure 4B–D) though cells were still round-shaped. HGFs on TNT30 and TNT-40 transformed to spindle shaped and extended tiny protrusions from the membrane into the opening of the nanotubes on the surfaces (Figure 4J and K). This kind of interaction resembled the natural insertion of collagen fibers in the connective tissue of gingiva. However, we did not understand from SEM images how deep these tiny protrusions from cell membrane were truly inserting into the nanotubes and whether collagen fibers would be secreted inside the nanotubes in an oriented pattern. This is one of the limitations that need further investigation in our future study.
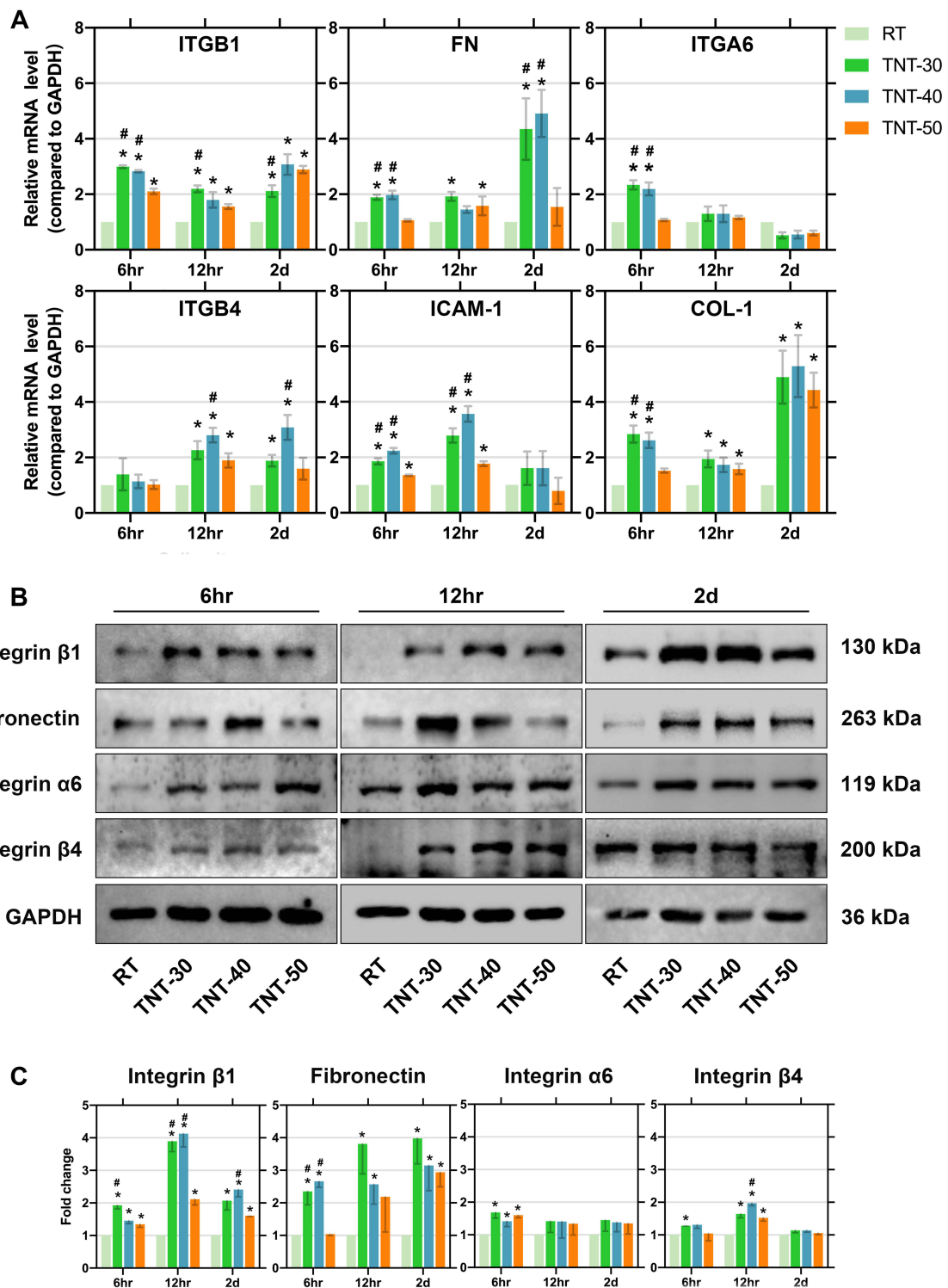
Figure 6 Gene and protein expression of adhesion molecules. The presence of nanotubes regulated adhesion-related gene expression of fibroblasts (**A**). It was noteworthy that integrin β1 (ITGB1) was upregulated, in all nanotube groups at all timepoints compared with RT (p<0.05). Fibronectin (FN) was upregulated in TNT-30 and 40 at 6 hr and 2 d of cell culture compared with RT and TNT-50 (p<0.05). Integrin α6 (ITGA6) was upregulated at 6 hr in TNT-30 and TNT-40 (p<0.05). At later stage of cell adhesion (12 hr and 2 d), Integrin β4 (ITGB4) was just upregulated in TNT30 and 40 (p<0.05). Intercellular cell adhesion molecule-1 (ICAM-1) was significantly upregulated in TNT-30 and 40 at 6 hr and 12 hr of cell culture compared with RT and TNT-50 (p<0.05). Gene expression of type I collagen was upregulated in TNT-30 and 40 at all timepoints of cell culture, compared with RT (p<0.05). Protein expression of Integrin β1/β4/α6 and fibronectin was evaluated via Western blot and the results of protein expression of adhesive molecule demonstrated that compared with the raw Ti, the presence of nanotubes on the surface exerted a positive role in regulating cell adhesion, especially the expression of integrin β1 and fibronectin at all the timepoints of cell culture (**B** and **C**). The presence of nanotubes surface increased the expression of integrin α6 at the initial 6th hour and integrin β4 at the 12th hour. At other timepoints, protein expression of integrin α6 and β4 was not significantly altered between groups. (*Represented p<0.05 compared with RT, #Represented p<0.05 compared with TNT-50).

Adhesion molecules are a group of cell surface components participating in various biological processes.[37,38] Integrin family has been widely recognized as a receptor and regulator on cell membrane, transducing cell signals from outer environment and motivating cell behaviors including cell proliferation, adhesion, and migration.[39–41] Integrin-mediated signal transduction regulates remodeling of cytoskeleton systems which plays an important role in cell movement, intracellular material transport, and the interaction with extracellular matrix (ECM). It was reported that actin-talin-integrin-fibronectin complex was developed to serve as a force sensor to transduce biochemical signals and regulate cell behaviors.[42] In the present work, we found fibronectin, integrin β1, β4, α6, and ICAM-1 in gene level was upregulated in nanotubes array groups at different timepoints compared with raw titanium disk. Besides, compared with disorderly nanotubes array (TNT-50), surface with highly ordered nanotubes array increased the expression of adhesion molecules (Figure 6A and C). However, we found no significant difference in gene and protein expression of adhesion molecules between TNT-30 and TNT-40 group which were both ordered array of nanotubes on Ti surfaces, indicating that tube diameter of 60 nm and 100 nm might not affect cell adhesion of gingival fibroblasts. The influence of pore diameter on cell growth and adhesion of HGFs are still controversial. For example, Gulati et al, found that nanopores with diameter of 50–75 nm on Ti surface increased cell area and cell aspect ratio compared with raw Ti but did not differ between groups of nanopores.[30] However, Ferrá-Cañellas et al, found that pore diameter of approximately 74 nm induced better HGFs response compared with pore size of 48 nm.[31] In the present work, we found Ti surfaces with highly ordered nanotubes (60 nm and 100 nm diameter) significantly enhanced HGFs cell adhesion at early phase compared with RT, while disordered array of nanotubes hindered cell adhesion, in spite of the large pore size (more than 100 nm) of some tubes found on the TNT-50 surface. To elucidate how pore size influences cell response of HGFs, in-depth investigation should be carried out in future studies.

Enhancing fiber secretion and further guiding oriented fibers inserting into the topographical structures on Ti-based materials have been two major challenges so far. It is worth noting that the gene expression of type I collagen (COL-1) was significantly upregulated in nanotubes groups, especially at the second day of cell culture (Figure 6A), indicating that nanotubes array might increase collagen secretion of fibroblasts accordingly. However, no inserting collagen fiber was found on the surface from SEM image in our in vitro assay, which was a drawback of present study. Chen et al, creatively inserted the type-I collagen into the nanotubes via semi-dry transfer system and successfully found perpendicular fibers protruded from the surface of Ti disks from second harmonic generation (SHG) microscopy.[43,44] But the work done was quite initial and there were still challenges before it could finally be used in clinical practices. Therefore, nanotubes array structures that are modified and optimized to accommodate the secreted collagen fibers of HGFs and to guide oriented fiber insertion would be very helpful for the integration of soft tissue sealing to the abutment surface of dental implant.

Conclusions

Tuning the Ti surface of the abutment of dental implants in a pattern advantageous for cell growth and adhesion of gingival fibroblasts (HGFs) and epithelium in the transmucosal region has been a recent focus in implant dentistry since a healthy cuff and tight sealing around the dental implant abutment is essential for resistance against incoming invasion of pathogenic microorganisms from the oral environment. Among various modifications, Ti surface with nanotubes fabricated via electrochemical anodization (EA) is attracting increasing attention due to its easy processing and tailorable topography, as well as the broader application in drug load and controlled release. In the present study, we found that compared with raw titanium surface, the presence of nanotubes array on titanium surface could significantly enhance HGFs adhesion and cell migration in the early phase. Additionally, compared with disorderly distributed nanotubes, highly ordered nanotubes array might provide a much more favorable surface for HGFs to achieve a tight adhesion on the materials. Gene and protein expression estimation confirmed upregulated expression in integrin family and intracellular adhesion molecules, suggesting improved cell adhesion of HGFs on the nanotubular surfaces. The fabricated surfaces containing nanotubes array might improve gingival adhesion and soft tissue healing around dental implant abutment, contributing to a tight sealing that is less fragile to dental implant diseases.

Abbreviations

COL-1, collagen type I; EA, electrochemical anodization; EDS, energy dispersive spectrum; FN, fibronectin; HD, hemidesmosome; HF, hydrofluoric acid; HF, hydrofluoric acid; HGFs, human gingival fibroblasts; ICAM-1, intercellular cell adhesion molecule-1; ITGA6, integrin α6; ITGB1, integrin β1; ITGB4, integrin β4; NH_4F, ammonium fluoride; SEM, scanning electron microscope; Ti, titanium; TNT, titanium nanotubes.

Ethics Approval and Informed Consent

The present study was approved and monitored by the ethics committee of the Fifth Affiliated Hospital of Sun Yat-sen University with ethics approval reference [2023-K207-1]. Informed consent was attained from the donators before the use of gingival fibroblast.

Author Contributions

All authors made a significant contribution to the work reported, whether that is in the conception, study design, execution, acquisition of data, analysis, and interpretation, or in all these areas; took part in drafting, revising, or critically reviewing the article; gave final approval of the version to be published; have agreed on the journal to which the article has been submitted; and agree to be accountable for all aspects of the work.

Funding

Disclosure

The authors declared no conflicts of interest in the present study.

References

1. Gibbs S, Roffel S, Meyer M, Gasser A. Biology of soft tissue repair: gingival epithelium in wound healing and attachment to the tooth and abutment surface. *Eur Cell Mater*. 2019;38:63–78. doi:10.22203/eCM.v038a06
2. Geurs NC, Vassilopoulos PJ, Reddy MS. Soft tissue considerations in implant site development. *Oral Maxillofac Surg Clin North Am*. 2010;22 (3):387–405, vi–vii. doi:10.1016/j.coms.2010.04.001
3. Atsuta I, Ayukawa Y, Kondo R, et al. Soft tissue sealing around dental implants based on histological interpretation. *J Prosthodont Res*. 2016;60 (1):3–11. doi:10.1016/j.jpor.2015.07.001
4. Wang Y, Zhang Y, Miron RJ. Health, maintenance, and Recovery of soft tissues around implants. *Clin Implant Dent Relat Res*. 2016;18 (3):618–634. doi:10.1111/cid.12343
5. Ivanovski S, Lee R. Comparison of peri-implant and periodontal marginal soft tissues in health and disease. *Periodontol 2000*. 2018;76(1):116–130. doi:10.1111/prd.12150
6. Canullo L, Genova T, Gross Trujillo E, et al. Fibroblast interaction with different abutment surfaces: in vitro study. *Int J Mol Sci*. 2020;21(6):1919. doi:10.3390/ijms21061919
7. Lee HJ, Lee J, Lee JT, et al. Microgrooves on titanium surface affect peri-implant cell adhesion and soft tissue sealing; an in vitro and in vivo study. *J Periodontal Implant Sci*. 2015;45(3):120–126. doi:10.5051/jpis.2015.45.3.120
8. Guo T, Gulati K, Arora H, Han P, Fournier B, Ivanovski S. Race to invade: understanding soft tissue integration at the transmucosal region of titanium dental implants. *Dent Mater*. 2021;37(5):816–831. doi:10.1016/j.dental.2021.02.005
9. Luchinskaya D, Du R, Owens DM, Tarnow D, Bittner N. Various surface treatments to implant provisional restorations and their effect on epithelial cell adhesion: a comparative in vitro study. *Implant Dent*. 2017;26(1):12–23. doi:10.1097/ID.0000000000000538
10. Andrukhov O, Behm C, Blufstein A, et al. Effect of implant surface material and roughness to the susceptibility of primary gingival fibroblasts to inflammatory stimuli. *Dent Mater*. 2020;36(6):e194–e205. doi:10.1016/j.dental.2020.04.003
11. Li D, Dai F, Li H, et al. Chitosan and collagen layer-by-layer assembly modified oriented nanofibers and their biological properties. *Carbohydr Polym*. 2021;254:117438. doi:10.1016/j.carbpol.2020.117438
12. Li Z, Du T, Gao C, et al. In-situ mineralized homogeneous collagen-based scaffolds for potential guided bone regeneration. *Biofabrication*. 2022;14 (4):045016. doi:10.1088/1758-5090/ac8dc7
13. Chen P, Liu L, Pan J, Mei J, Li C, Zheng Y. Biomimetic composite scaffold of hydroxyapatite/gelatin-chitosan core-shell nanofibers for bone tissue engineering. *Mater Sci Eng C Mater Biol Appl*. 2019;97:325–335. doi:10.1016/j.msec.2018.12.027
14. Hotchkiss KM, Reddy GB, Hyzy SL, Schwartz Z, Boyan BD, Olivares-Navarrete R. Titanium surface characteristics, including topography and wettability, alter macrophage activation. *Acta Biomater*. 2016;31:425–434. doi:10.1016/j.actbio.2015.12.003
15. Kartikasari N, Yamada M, Watanabe J, et al. Titanium surface with nanospikes tunes macrophage polarization to produce inhibitory factors for osteoclastogenesis through nanotopographic cues. *Acta Biomater*. 2022;137:316–330. doi:10.1016/j.actbio.2021.10.019

16. Ferraris S, Truffa Giachet F, Miola M, et al. Nanogrooves and keratin nanofibers on titanium surfaces aimed at driving gingival fibroblasts alignment and proliferation without increasing bacterial adhesion. *Mater Sci Eng C Mater Biol Appl*. 2017;76:1–12. doi:10.1016/j.msec.2017.02.152

17. Gulati K, Santos A, Findlay D, Losic D. Optimizing anodization conditions for the growth of titania nanotubes on curved surfaces. *J Phys Chem C*. 2015;119(28):16033–16045. doi:10.1021/acs.jpcc.5b03383

18. Lai M, Jin Z, Su Z. Surface modification of TiO(2) nanotubes with osteogenic growth peptide to enhance osteoblast differentiation. *Mater Sci Eng C Mater Biol Appl*. 2017;73:490–497. doi:10.1016/j.msec.2016.12.083

19. Zhao X, You L, Wang T, et al. Enhanced osseointegration of titanium implants by surface modification with silicon-doped titania nanotubes. *Int J Nanomed*. 2020;15:8583–8594. doi:10.2147/IJN.S270311

20. Somsanith N, Kim YK, Jang YS, et al. Enhancing of osseointegration with propolis-loaded TiO(2) nanotubes in rat mandible for dental implants. *Materials*. 2018;11(1):61. doi:10.3390/ma11010061

21. Gao H, Jiang N, Niu Q, Mei S, Haugen HJ, Ma Q. Biocompatible nanostructured silver-incorporated implant surfaces show effective antibacterial, osteogenic, and anti-inflammatory effects in vitro and in rat model. *Int J Nanomed*. 2023;18:7359–7378. doi:10.2147/IJN.S435415

22. Gulati K, Ivanovski S. Dental implants modified with drug releasing titania nanotubes: therapeutic potential and developmental challenges. *Expert Opin Drug Deliv*. 2017;14(8):1009–1024. doi:10.1080/17425247.2017.1266332

23. Mei S, Wang H, Wang W, et al. Antibacterial effects and biocompatibility of titanium surfaces with graded silver incorporation in titania nanotubes. *Biomaterials*. 2014;35(14):4255–4265. doi:10.1016/j.biomaterials.2014.02.005

24. Forstater JH, Kleinhammes A, Wu Y. Self-assembly of protein-based biomaterials initiated by titania nanotubes. *Langmuir*. 2013;29(48):15013–15021. doi:10.1021/la403414t

25. Fu Y, Jing Z, Chen T, et al. Nanotube patterning reduces macrophage inflammatory response via nuclear mechanotransduction. *J Nanobiotechnology*. 2023;21(1):229. doi:10.1186/s12951-023-01912-4

26. He Y, Li Z, Ding X, et al. Nanoporous titanium implant surface promotes osteogenesis by suppressing osteoclastogenesis via integrin beta1/FAKpY397/MAPK pathway. *Bioact Mater*. 2022;8:109–123. doi:10.1016/j.bioactmat.2021.06.033

27. Li D, Yang L, Deng H, Li T, Zhang Z. Optimized titanium dioxide nanotubes for dental implants: estimation of mechanical properties and effects on the biological behaviors of human gingival fibroblasts and oral bacteria. *J Mech Behav Biomed Mater*. 2023;144:105988. doi:10.1016/j.jmbbm.2023.105988

28. Crenn M-J, Dubot P, Mimran E, Fromentin O, Lebon N, Peyre P. Influence of anodized titanium surfaces on the behavior of gingival cells in contact with: a systematic review of in vitro studies. *Crystals*. 2021;11(12):1566. doi:10.3390/cryst11121566

29. Palkowitz AL, Tuna T, Bishti S, et al. Biofunctionalization of dental abutment surfaces by crosslinked ECM proteins strongly enhances adhesion and proliferation of gingival fibroblasts. *Adv Healthc Mater*. 2021;10(10):e2100132. doi:10.1002/adhm.202100132

30. Gulati K, Moon HJ, Kumar PTS, Han P, Ivanovski S. Anodized anisotropic titanium surfaces for enhanced guidance of gingival fibroblasts. *Mater Sci Eng C Mater Biol Appl*. 2020;112:110860. doi:10.1016/j.msec.2020.110860

31. Ferra-Canellas MDM, Llopis-Grimalt MA, Monjo M, Ramis JM. Tuning nanopore diameter of titanium surfaces to improve human gingival fibroblast response. *Int J Mol Sci*. 2018;19(10):2881. doi:10.3390/ijms19102881

32. Wang C, Wang X, Lu R, Gao S, Ling Y, Chen S. Responses of human gingival fibroblasts to superhydrophilic hydrogenated titanium dioxide nanotubes. *Colloids Surf B Biointerfaces*. 2021;198:111489. doi:10.1016/j.colsurfb.2020.111489

33. Ahamed AS, Prakash PSG, Crena J, Victor DJ, Subramanian S, Appukuttan D. The influence of laser-microgrooved implant and abutment surfaces on mean crestal bone levels and peri-implant soft tissue healing: a 3-year longitudinal randomized controlled clinical trial. *Int J Implant Dent*. 2021;7(1):102. doi:10.1186/s40729-021-00382-3

34. Plikus MV, Wang X, Sinha S, et al. Fibroblasts: origins, definitions, and functions in health and disease. *Cell*. 2021;184(15):3852–3872. doi:10.1016/j.cell.2021.06.024

35. Smith PC, Martinez C, Martinez J, McCulloch CA. Role of fibroblast populations in periodontal wound healing and tissue remodeling. *Front Physiol*. 2019;10:270. doi:10.3389/fphys.2019.00270

36. Green KJ, Getsios S, Troyanovsky S, Godsel LM. Intercellular junction assembly, dynamics, and homeostasis. *Cold Spring Harb Perspect Biol*. 2010;2(2):a000125. doi:10.1101/cshperspect.a000125

37. Honig B, Shapiro L. Adhesion protein structure, molecular affinities, and principles of cell-cell recognition. *Cell*. 2020;181(3):520–535. doi:10.1016/j.cell.2020.04.010

38. Walko G, Castanon MJ, Wiche G. Molecular architecture and function of the hemidesmosome. *Cell Tissue Res*. 2015;360(2):363–378. doi:10.1007/s00441-014-2061-z

39. Bachmann M, Kukkurainen S, Hytonen VP, Wehrle-Haller B. Cell adhesion by integrins. *Physiol Rev*. 2019;99(4):1655–1699. doi:10.1152/physrev.00036.2018

40. Hood JD, Cheresh DA. Role of integrins in cell invasion and migration. *Nat Rev Cancer*. 2002;2(2):91–100. doi:10.1038/nrc727

41. Litjens SH, de Pereda JM, Sonnenberg A. Current insights into the formation and breakdown of hemidesmosomes. *Trends Cell Biol*. 2006;16(7):376–383. doi:10.1016/j.tcb.2006.05.004

42. Elosegui-Artola A, Oria R, Chen Y, et al. Mechanical regulation of a molecular clutch defines force transmission and transduction in response to matrix rigidity. *Nat Cell Biol*. 2016;18(5):540–548. doi:10.1038/ncb3336

43. Chen CY, Kim DM, Lee C, et al. Biological efficacy of perpendicular type-I collagen protruded from TiO2-nanotubes. *Int J Oral Sci*. 2020;12(36). doi:10.1038/s41368-020-00103-3

44. Nojiri T, Chen CY, Kim DM, et al. Establishment of perpendicular protrusion of type I collagen on TiO2 nanotube surface as a priming site of peri-implant connective fibers. *J Nanobiotechnology*. 2019;17(1):34. doi:10.1186/s12951-019-0467-1